Identification and validation of three diagnostic autophagy-related genes associated with advanced plaques and immune cell infiltration in carotid atherosclerosis based on integrated bioinformatics analyses

Tiegen Huang[1], Chen Su[1], Quanli Su[1], Yali Nie[1], Zhenni Xiao[1], Yao Tang[1], Jiahao Wang[1], Xiaotian Luo[1] and Yixin Tang[1,2]

[1] Hengyang Medical School, University of South China, The First Affiliated Hospital, Department of Cardiology, Hengyang, Hunan, China
[2] University of South China, Hunan Provincial Key Laboratory of Multi-omics and Artificial Intelligence of Cardiovascular Diseases, Hengyang, Hunan, China

ABSTRACT

Background: Autophagy plays a key role in the development of carotid atherosclerosis (CAS). This study aimed to identify key autophagy-related genes (ATGs) related with CAS using bioinformatics analysis, *in vivo* AS mouse model, and *in vitro* experiments.

Methods: The GSE100927 and GSE28829 datasets were downloaded from the Gene Expression Omnibus (GEO) database. An integrated bioinformatics analyses of differentially expressed ATGs (DE-ATGs) was conducted. Gene ontology (GO) and Kyoto Encyclopedia of Genes and Genomes (KEGG) enrichment analyses were performed to identify the biological processes and pathways associated with DE-ATGs. Protein-protein interaction (PPI) network was constructed with the DE-ATGs to identify the key CAS-related DE-ATGs. Receiver operating characteristic (ROC) curve analysis was used to determine the diagnostic value of the key CAS-related DE-ATGs. CIBERSORT analysis was performed to determine the infiltration status of 22 immune cell types and their correlation with the expression levels of the key CAS-related DE-ATGs. Hematoxylin and eosin (HE) staining was used to estimate the plaque histology in the AS mouse model. Western blotting, quantitative real-time PCR (qRT-PCR), and immunohistochemistry (IHC) were performed to validate the protein and mRNA expression levels of the key CAS-related DE-ATGs in the *in vitro* and *in vivo* models.

Results: We compared transcriptome profiles of 12 early CAS plaques and 29 advanced CAS plaques in the GSE100927 dataset and identified 41 DE-ATGs (33 up-regulated and eight down-regulated). Functional enrichment analysis showed that the DE-ATGs were closely related with apoptosis, autophagy, and immune activation. ROC curve analysis showed that the area under the curve (AUC) values for the three key CAS-related DE-ATGs (*CCL2*, *LAMP2*, and *CTSB*) were 0.707, 0.977, and 0.951, respectively. CIBERSORT analyses showed close association between the three key CAS-related DE-ATGs and the infiltration of immune cell

Submitted 4 July 2024
Accepted 28 October 2024
Published 22 November 2024

Corresponding authors
Xiaotian Luo, 276322293@qq.com
Yixin Tang, tytangyixin2014@sina.com

Academic editor
Steven Buyske

Additional Information and Declarations can be found on page 16

DOI **10.7717/peerj.18543**

How to cite this article Huang T, Su C, Su Q, Nie Y, Xiao Z, Tang Y, Wang J, Luo X, Tang Y. 2024. Identification and validation of three diagnostic autophagy-related genes associated with advanced plaques and immune cell infiltration in carotid atherosclerosis based on integrated bioinformatics analyses. **PeerJ 12:e18543 DOI 10.7717/peerj.18543**

types in the plaques. Finally, the western blot, qRT-PCR, and IHC staining confirmed that CCL2, LAMP2, and CTSB were highly expressed in the plaques of the AS model mice or ox-LDL-treated human umbilical vein endothelial cells (HUVECs) and human aorta vascular smooth muscle cells (HAoSMCs).
Conclusion: We identified and validated three key CAS-associated ATGs, namely, *CCL2*, *LAMP2*, and *CTSB* with high diagnostic value. These three key CAS-associated ATGs are promising diagnostic markers and therapeutic targets for patients with CAS.

Subjects Genetics, Genomics, Cardiology
Keywords Carotid atherosclerosis, Autophagy, Immune cell infiltration, Bioinformatics analyses, Immunohistochemistry

INTRODUCTION

Carotid atherosclerosis (CAS) is a chronic inflammatory disease of the carotid artery (*Kong et al., 2022*; *Stary et al., 1995*; *Tedgui & Mallat, 2006*) and plays a vital role in the cerebral ischemic events, including ischemic strokes (*Bos et al., 2021*; *Saba et al., 2019*). The pathophysiology of CAS is not clearly established. However, several studies have shown that CAS is linked with inflammation, lipid metabolism disorders, as well as dysfunction of the endothelial cells and smooth muscle cells (*Lu & Daugherty, 2015*). Autophagy plays a critical role in the development of CAS, but the precise mechanism by which autophagy regulates CAS development and progression is unclear.

Autophagy is a process of self-eating in which damaged cellular proteins and organelles are degraded in the lysosomes; this process is regulated by the autophagy-related genes (ATGs) (*Grootaert et al., 2018*; *Levine & Kroemer, 2019*). Autophagy is categorized into three types: chaperone-mediated autophagy, microautophagy, and macroautophagy (*Mahapatra et al., 2021*). Autophagy dysregulation is implicated in the pathogenesis of inflammatory diseases, neurodegenerative diseases, cancers, and autoimmune disorders (*Mizushima & Levine, 2020*; *Yamamoto, Zhang & Mizushima, 2023*).

Autophagy maintains intracellular homeostasis of several cardiovascular cell types, including the vascular smooth muscle cells (VSMCs) and endothelial cells (*Bravo-San Pedro, Kroemer & Galluzzi, 2017*). Several studies have demonstrated that aberrant expression of several ATGs is significantly associated with the progression of CAS. For example, ATG7 silencing in the VSMCs and mice inhibited autophagy and accelerated atherosclerotic development (*Osonoi et al., 2018*). Furthermore, defective autophagy accelerated atherosclerosis in the ATG5 knockout macrophages and mice (*Liao et al., 2012*).

Ischemic stroke (IS) is one of the major causes of disability worldwide. IS is mainly caused by CAS. Carotid endarterectomy and stenting are well-established clinical procedures for preventing ischemic stroke (*Masuhr & Busch, 2004*; *Zhu et al., 2022*). However, recent advances in technology have resulted in the emergence of alternative approaches such as nanocarriers (*Azadi et al., 2021*), stem cell therapy (*Ma et al., 2023*), and neural repair (*Chopp, Li & Zhang, 2009*) for preventing stroke or effective treatment of

patients with CAS. Carotid endarterectomy is associated with a significant risk of postoperative complications, and early intervention of CAS involves a high procedural cost. Therefore, there is an urgent need of developing highly effective diagnostic biomarkers for the early indication of CAS. Several studies have demonstrated the significance of autophagy in CAS. However, autophagic biomarkers with clinical importance for the early detection, prognosis, and treatment of CAS have not been established.

This study performed in-depth bioinformatics analysis of the transcriptome data from the early and advanced CAS plaques to identify key differentially expressed ATGs (DE-ATGs) that were associated with CAS progression. We also assessed the relationship between the key CAS-related DE-ATGs and the immune cells. We also investigated the diagnostic value of the key CAS-related DE-ATGs. The expression levels of the key CAS-related DE-ATGs were further validated in the *in vitro* and *in vivo* experiments.

MATERIALS AND METHODS

Data acquisition and processing

We acquired 222 autophagy-related genes (ATGs) from the human autophagy database (http://www.autophagy.lu/index.html). Two CAS mRNA expression profiles (GSE100927 and GSE28829) were downloaded from the GEO database (http://www.ncbi.nlm.nih.gov/geo/). The GSE100927 dataset was based on the GPL17077 platform (Agilent-039494 SurePrint G3 Human GE v2 8x60K Microarray 039381) and consisted of 35 early plaques and 69 advanced plaques. We chose 12 early CAS plaques and 29 advanced CAS plaques from the GSE100927 dataset for our analysis (*Steenman et al., 2018*). The GSE28829 dataset was based on the GPL570 platform (Affymetrix Human Genome U133 Plus 2.0 Array) and consisted of 13 early CAS plaques and 16 advanced CAS plaques. Sample collection and processing for GSE100927 and GSE28829 were performed in accordance with the guidelines of the guidelines of the Medical and Ethical Committee in Nantes, France and the Code for Proper Secondary Use of Human Tissue, respectively, and written informed consent was obtained from all patients and from next of kin for all organ donors. The probe IDs in the expression matrix were processed into gene symbols using the annotation file in the gene chip.

Identification of differentially expressed ATGs (DE-ATGs)

Principal component analysis (PCA) was performed using the "FactoMineR" and "factoextra" packages. The differentially expressed genes were identified between early and advanced atherosclerotic plaques using the "limma" package with $|\log2FC| > 0.5$ and P-value < 0.05 as the threshold parameters. The heatmap, volcano plots, and boxplots were generated with the "heatmap" and "ggplot2" packages. The DE-ATGs were identified by taking intersections of the DEGs with the 222 ATGs through an online web tool (https://bioinformatics.psb.ugent.be/webtools/Venn/).

Functional enrichment analysis of DE-ATGs

GO and KEGG enrichment analyses of the DE-ATGs were performed using the "clusterProfiler" and "GOplot" packages in the R software and the results were visualized using bubble plots and the chord diagram.

Protein-protein interaction (PPI) analysis and identification of key CAS-related DE-ATGs

PPI network of the DE-ATGs was constructed using the STRING online database (https://string-db.org/). Interactions between the DE-ATGs were visualized using the Cytoscape software (version 3.9.1). The key CAS-related DE-ATGs were extracted using the cytoHubba plugin. The GSE28829 dataset was used to validate the statistical significance of these key CAS-related DE-ATGs in the early and advanced CAS plaques.

Diagnostic value of the key CAS-related DE-ATGs

The "pROC" package was used to test the diagnostic value of these key CAS-related DE-ATGs in the GSE100927 dataset. Furthermore, the logistic regression model of the key DE-ATGs was generated and tested using the GSE100927 dataset. The GSE28829 dataset was used as the external validation dataset.

Immune cell infiltration analysis

CIBERSORT is a bioinformatic tool to determine the cellular composition of tissues based on their gene expression profiles (*Ke et al., 2024*). The proportion of 22 immune cell types, including B cells, T cells, macrophages, and NK cells, in the early and advanced CAS samples of GSE100927 were analyzed with CIBERSORT using the LM22 signature matrix as reference (*Newman et al., 2015*). We performed up to 1,000 permutations and retained samples with $P < 0.05$ to ensure accuracy of the results. The sum of various immune cells was set as 1. The results from CIBERSORT were visualized using the ggbarplot, ggplot2, ggcorrplot, and heatmap R packages.

Cell culture

Human umbilical vein endothelial cells (HUVECs; AW-CNH488) and human aorta vascular smooth muscle cells (HAoSMCs; AW-YCH013) were purchased for this study from Abiowell Biotechnology Co. Ltd (Changsha, China). HUVECs and HAoSMCs were grown in Dulbecco's Modified Eagle Medium (105690010; Gibco, Grand Island, NY, USA) at 37 °C and 5% CO_2 in a humidified incubator. The cells in the AS group were treated with 50 μg/mL ox-LDL (YB-002; Yiyuan Biotechnologies, Guangzhou, China) for 24 h after they reached 70–80% confluence. The cells grown in normal medium were regarded as the control group.

Western blotting

The cells were lysed in the RIPA buffer (SL1020; Coolaber, Bernards, NJ, USA) and the protein lysates were quantified. Equal amounts of protein lysates were electrophoresed on the SDS-PAGE. The separated proteins were transferred onto the PVDF membranes. The membranes were blocked with 5% skimmed milk for 1 h at room temperature.

Subsequently, the membranes were incubated overnight at 4 °C with the following rabbit polyclonal primary antibodies against CCL2 (A7277; Abclonal, Woburn, MA, USA), LAMP2 (ab199947; Abcam, Cambridge, UK), CTSB (12216-1-AP; Proteintech, Rosemont, IL, USA), and β-actin (20536-1-AP; Proteintech, Rosemont, IL, USA). Then, the membranes were incubated with the anti-rabbit IgG-HRP antibody (A21020; Abbkine, Atlanta, GA, USA). The protein band signals were developed using the ECL Detection System (WBKLS0500; Merck Millipore, Burlington, MA, USA).

Quantitative real-time PCR (qRT-PCR)

Total RNA samples were prepared using the Trizol reagent (15596026; Invitrogen, Waltham, MA, USA). Then, cDNA was generated from the total RNA using the RevertAid First Strand cDNA Synthesis Kit (K1622; Thermofisher, Waltham, MA, USA). Real-time qPCR was performed using the SYBR Green Master Mix (11201ES08; Yeasen Biotechnology, Shanghai, China). The individual mRNA expression levels were normalized to GAPDH. All the primer sequences are listed in Table S1.

Animals

All animal experiments were approved by the Animal Care and Use Committee of the University of South China (permission No. USC2023XS085) and conducted in accordance with the National Institutes of Health Guide. Six male 8-week-old ApoE$^{-/-}$ mice on a C57BL/6J background and six wild-type C57BL/6J mice were purchased from the Vital River Laboratory Animal Center (Beijing, China) and housed under a 12 h light/dark cycle with free access to drinking water and food in an environmentally controlled room (20–26 °C, 60% humidity). Among these, six wild-type C57BL/6J mice fed on normal chow diet containing 4% fat and 0% cholesterol were considered as the control group, and six ApoE$^{-/-}$ mice fed on a Western diet containing 20% fat and 1.25% cholesterol were considered as the AS group. After 12 weeks, the experimental mice were euthanized by CO_2 asphyxiation. Stack experimental animals in the euthanasia box, and introduce CO_2 to the animal. There were no mice left in this study and were used for experiments. The mice were anaesthetized and sacrificed for collection of aortic tissue and follow-up examinations.

Oil Red O (ORO) staining

The entire aorta from the ascending aorta to the bifurcation of the iliac arteries was isolated, stripped of peripheral vascular fat, and incised longitudinally. Then, it was stained with the ORO dye (G1015; Servicebio, Hubei, China) and photographed with a digital camera. The percentage of area occupied by the ORO-positive area was assessed using the ImageJ software (NIH).

Hematoxylin and eosin (HE) staining

The aortic root tissue was fixed with 4% PFA (G1101; Servicebio, Hubei, China), embedded in paraffin, and sectioned. The sections were baked in the oven, deparaffinized, hematoxylin-stained, eosin-stained, dehydrated in alcohol, placed in xylene, sealed with a

cover slip, and observed under the microscope. The aortic root plaque area was quantified by ImageJ software.

Immunohistochemistry (IHC) staining

The sections of aortic root tissue samples were baked in an oven and deparaffinized. Subsequently, the sections were subjected to antigen retrieval at high temperature and incubated with 3% hydrogen peroxide. The sections were incubated with rabbit polyclonal primary antibodies against CCL2 (A7277; Abclonal, Woburn, MA, USA), LAMP2 (ab199947; Abcam, Cambridge, UK), and CTSB (12216-1-AP; Proteintech, Rosemont, IL, USA). Then, the sections were incubated with the anti-rabbit IgG polymer (PV-9001; ZSGB-Bio, Beijing, China). The sections were then incubated with the DAB working solution (ZLI-9018; ZSGB-Bio, Beijing, China), counterstained with hematoxylin, dehydrated in alcohol, placed in xylene, and finally sealed with a coverslip. The stained sections were observed and photographed under the microscope. ImageJ software was used to quantify the ratio of the yellow-positive area to the aortic root plaque area.

Statistical analysis

Statistical analysis was performed using the GraphPad Prism 9 software and R software (version 4.3.0). Student's t-test was used to determine statistical significance between groups. P-value < 0.05 was considered statistically significant.

RESULTS

Identification of CAS-related DE-ATGs

The study's overall flowchart is presented in Fig. 1. Principal component analysis (PCA) was performed to compare the CAS and control groups in the GSE100927 dataset. We obtained two distinct groups with significant differences (Fig. 2A). Our data showed upregulation of 1,973 genes and downregulation of 1,590 genes in the CAS group compared with the control group (Fig. 2B). Furthermore, overlapping of these DEGs with the 222 ATGs resulted in the identification of 41 DE-ATGs (33 upregulated and eight down-regulated ATGs) (Fig. 2C). The heatmap of DE-ATGs in different samples is shown in Fig. 2D. Boxplots showed the differences in the gene expression levels of 41 DE-ATGs in the CAS and control samples. The top five up-regulated genes were CTSB, CTSD, CXCR4, SERPINA1, and RGS19; and the top five downregulated genes were HSPB8, EGFR, NCKAP1, ERBB2, and CX3CL1 (Figs. 3A and 3B).

Functional enrichment analysis of DE-ATGs

GO enrichment analyses showed that the top biological process associated with the DE-ATGs were regulation of endopeptidase activity, macroautophagy, and regulation of autophagy; the top cellular component were membrane raft, membrane microdomain, and vacuolar membrane; the top molecular functions were cytokine receptor binding and virus receptor activity (Fig. 4A; Table S2). KEGG pathway enrichment analyses showed that the top KEGG pathways associated with the DE-ATGs were NOD-like receptor signaling pathway, apoptosis, autophagy, and immune activation (Fig. 4B; Table S3). In summary,

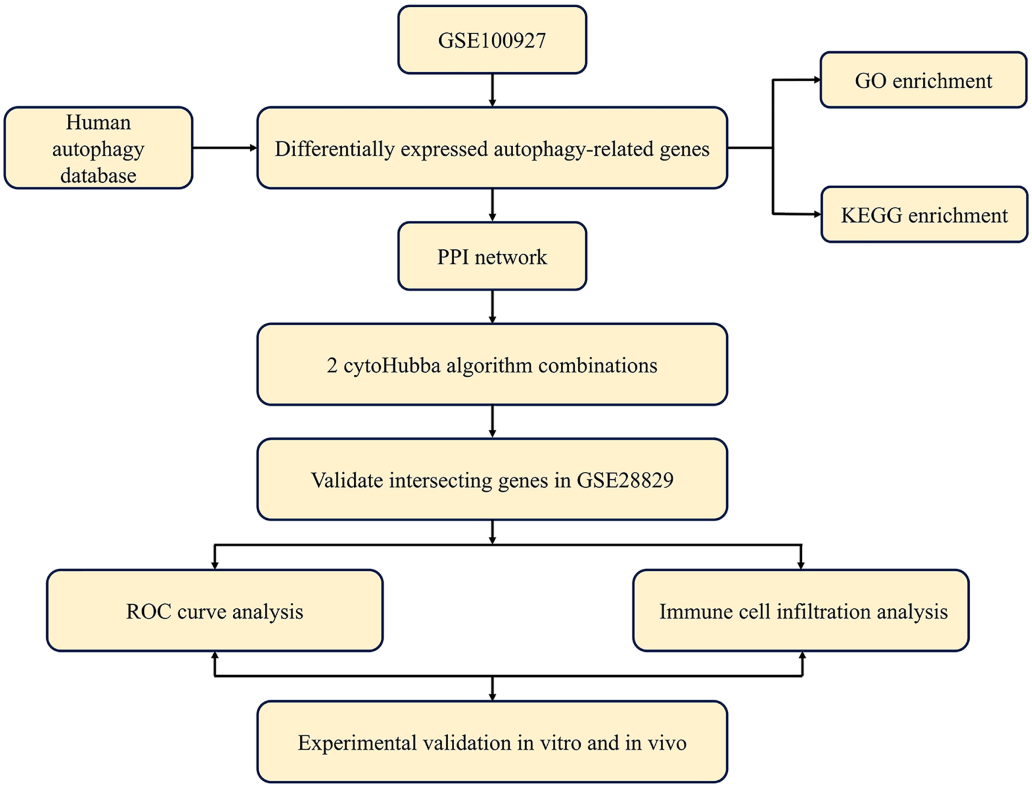

Figure 1 **Overall flowchart of this study.** Full-size DOI: 10.7717/peerj.18543/fig-1

the CAS-related DE-ATGs were associated with apoptosis, autophagy, and immune activation.

PPI network and screening of key CAS-related DE-ATGs with diagnostic significance

Figure 5A shows the PPI network between the CAS-related DE-ATGs. We identified the top 10 key CAS-related DE-ATGs using the MCC and BottleNeck algorithms of the "cytoHubba" plugin (Figs. 5B and 5C). Subsequently, we identified seven key CAS-related DE-ATGs after taking the intersection (Fig. 5D). We then performed validation analyses using the GSE28829 dataset and identified that the expression levels of *LAMP1*, *CASP8*, *FOS*, and *EGFR* did not show statistically significant differences (Fig. 5E). Finally, we identified *CCL2*, *LAMP2*, and *CTSB* as three key CAS-related DE-ATGs that were potentially involved in the pathogenesis of CAS.

Diagnostic value of key CAS-related DE-ATGs

ROC curve analysis confirmed that *CCL2*, *LAMP2*, and *CTSB* showed good diagnostic performances in discriminating between CAS and control samples with AUC values of 0.707, 0.977, and 0.951, respectively (Figs. 6A–6C). The diagnostic values of the three key CAS-related DE-ATGs were validated in the GSE28829 dataset and showed AUC values of 0.760, 0.827, and 0.947 for *CCL2*, *LAMP2*, and *CTSB* respectively (Fig. 6D). This demonstrated high diagnostic performance of *CCL2*, *LAMP2*, and *CTSB* for discriminating

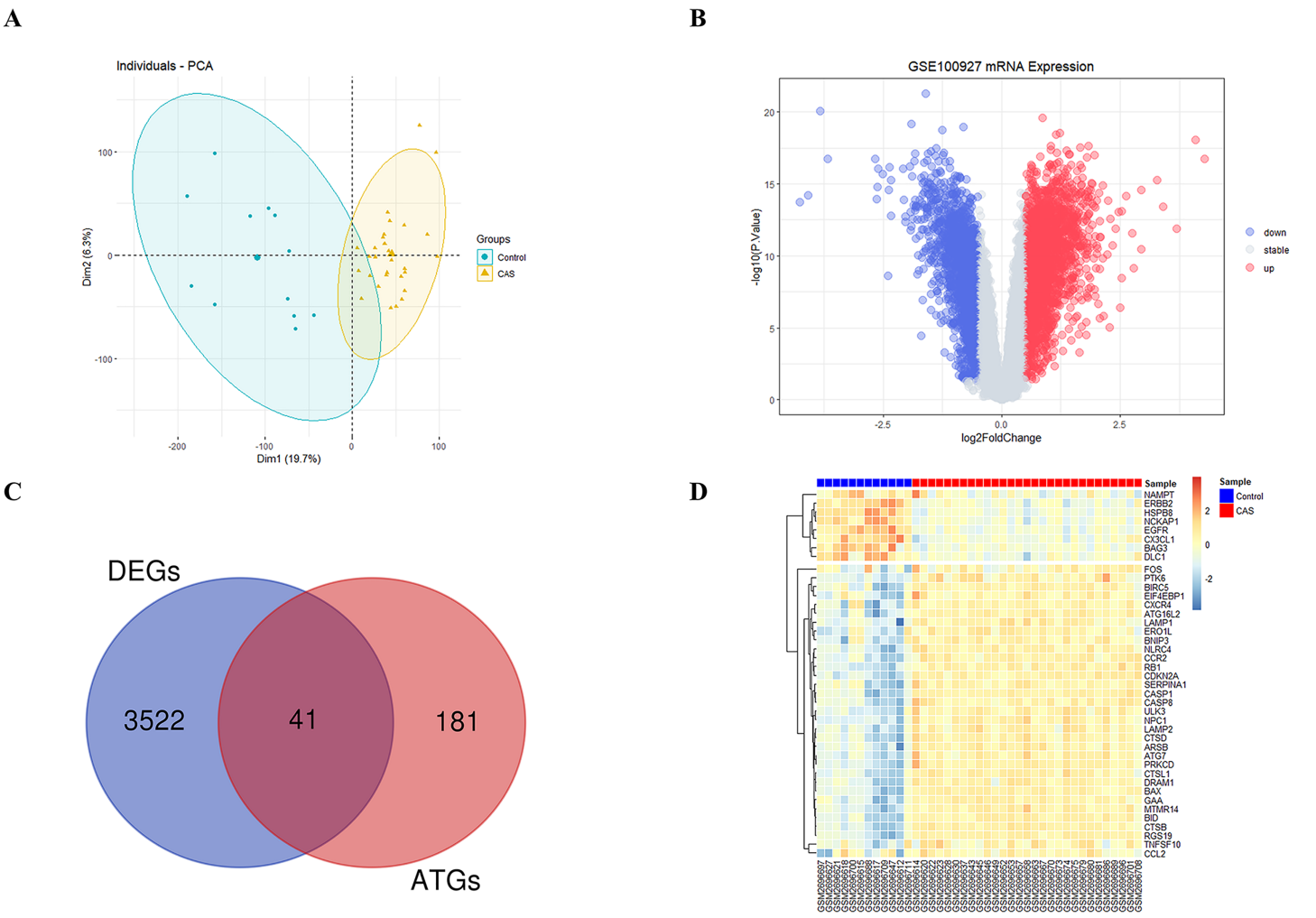

Figure 2 The DE-ATGs in CAS and control samples. (A) PCA for GSE100927. (B) The volcano plot of GSE100927, (C) the Venn plot and (D) the heatmap of DE-ATGs.
Full-size DOI: 10.7717/peerj.18543/fig-2

late CAS from early CAS. Based on the logistic regression model, AUC values for the GSE100927 and GSE28829 datasets were 0.994 and 0.981, respectively (Figs. 6E and 6F).

Immune infiltration

CIBERSORT analyses showed that the proportion of immune cells was significantly different between the early CAS plaques and the advanced CAS plaques (Fig. 7A). The proportion of memory B cells, gamma delta T cells, M0 macrophages, and activated mast cells was significantly higher in the advanced CAS plaques (Fig. 7B). Subsequently, we analyzed the correlation between the 22 types of immune cells in the plaques and observed that most of the immune cell types were significantly associated with each other. Naive B cells and resting NK cells showed the most synergistic effect, whereas gamma delta T cells and resting memory CD4 T cells showed the most competitive effect (Fig. 8A). Furthermore, the expression levels of *CCL2*, *LAMP2*, and *CTSB* showed close association with the infiltration levels of the immune cells (Fig. 8B). These data demonstrated that

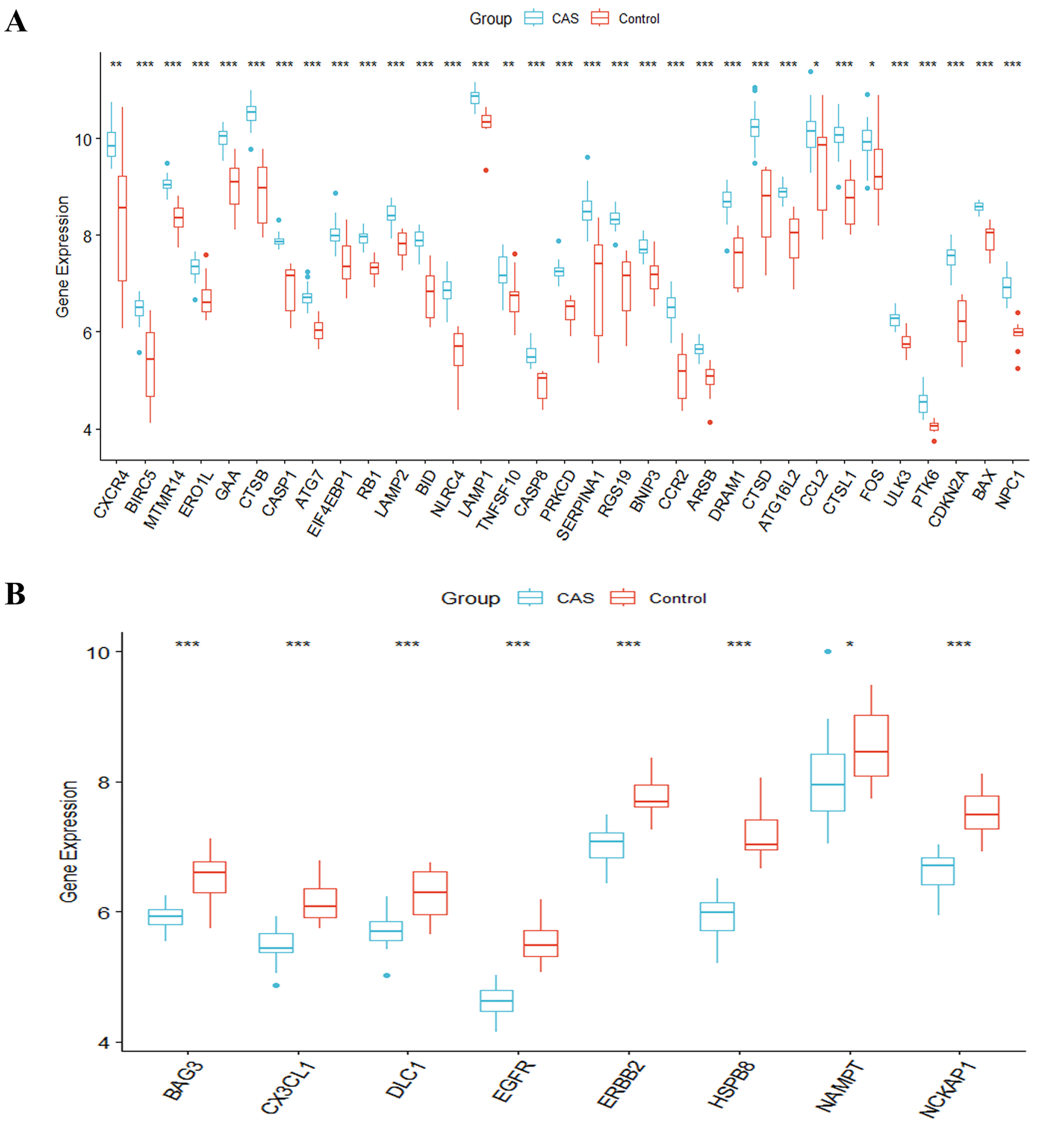

Figure 3 The boxplot of 41 DE-ATGs. (A) The boxplot of 33 up-regulated DE-ATGs. (B) The boxplot of eight down-regulated DE-ATGs. *$P < 0.05$; **$P < 0.01$; ***$P < 0.001$.

Full-size DOI: 10.7717/peerj.18543/fig-3

activation of autophagy was associated with increased inflammatory responses during the progression of CAS.

Validation of key CAS-related DE-ATGs using *in vitro* and *in vivo* models

The treatment of HUVECs and HAoSMCs with ox-LDL significantly increased the expression levels of CCL2, LAMP2, and CTSB proteins (Figs. 9A and 9B) and mRNAs (Fig. 9C). Furthermore, ORO staining results demonstrated significant increase in the levels of atherosclerotic lesions in the high-fat-fed ApoE$^{-/-}$ mice compared with the control group (Figs. 9D and 9G). Moreover, H&E staining results showed larger plaques in the aortic root of the high-fat-fed ApoE$^{-/-}$ mice compared with normal-diet-fed C57BL/6

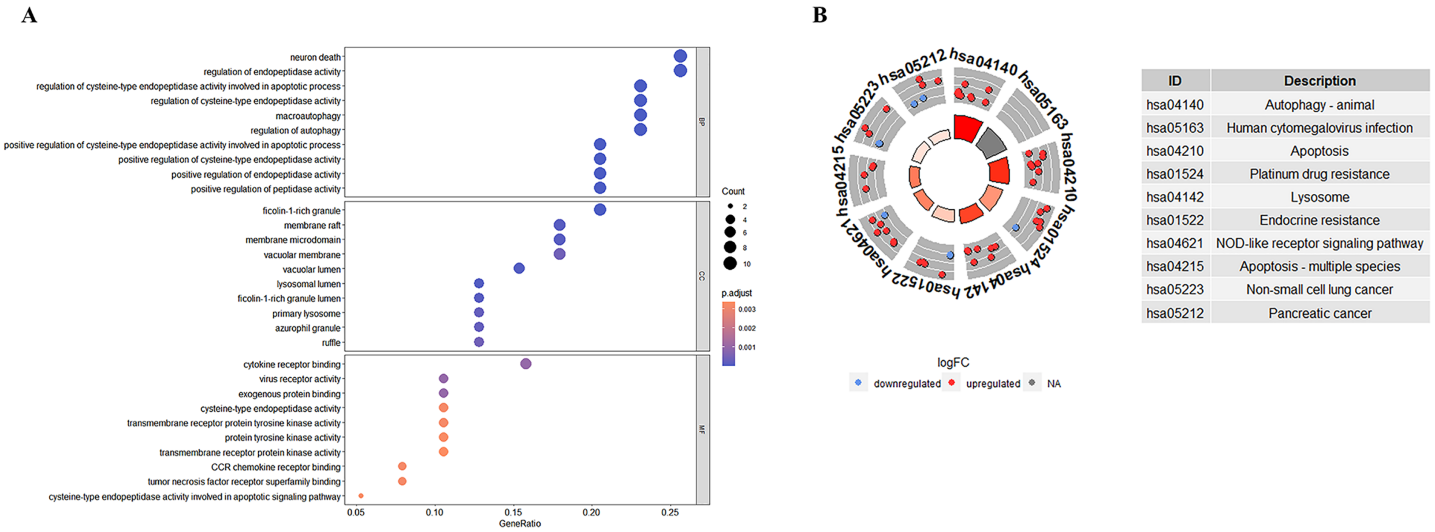

Figure 4 GO and KEGG enrichment analysis of 41 DE-ATGs. (A) GO enrichment analysis. (B) KEGG enrichment analysis.
Full-size DOI: 10.7717/peerj.18543/fig-4

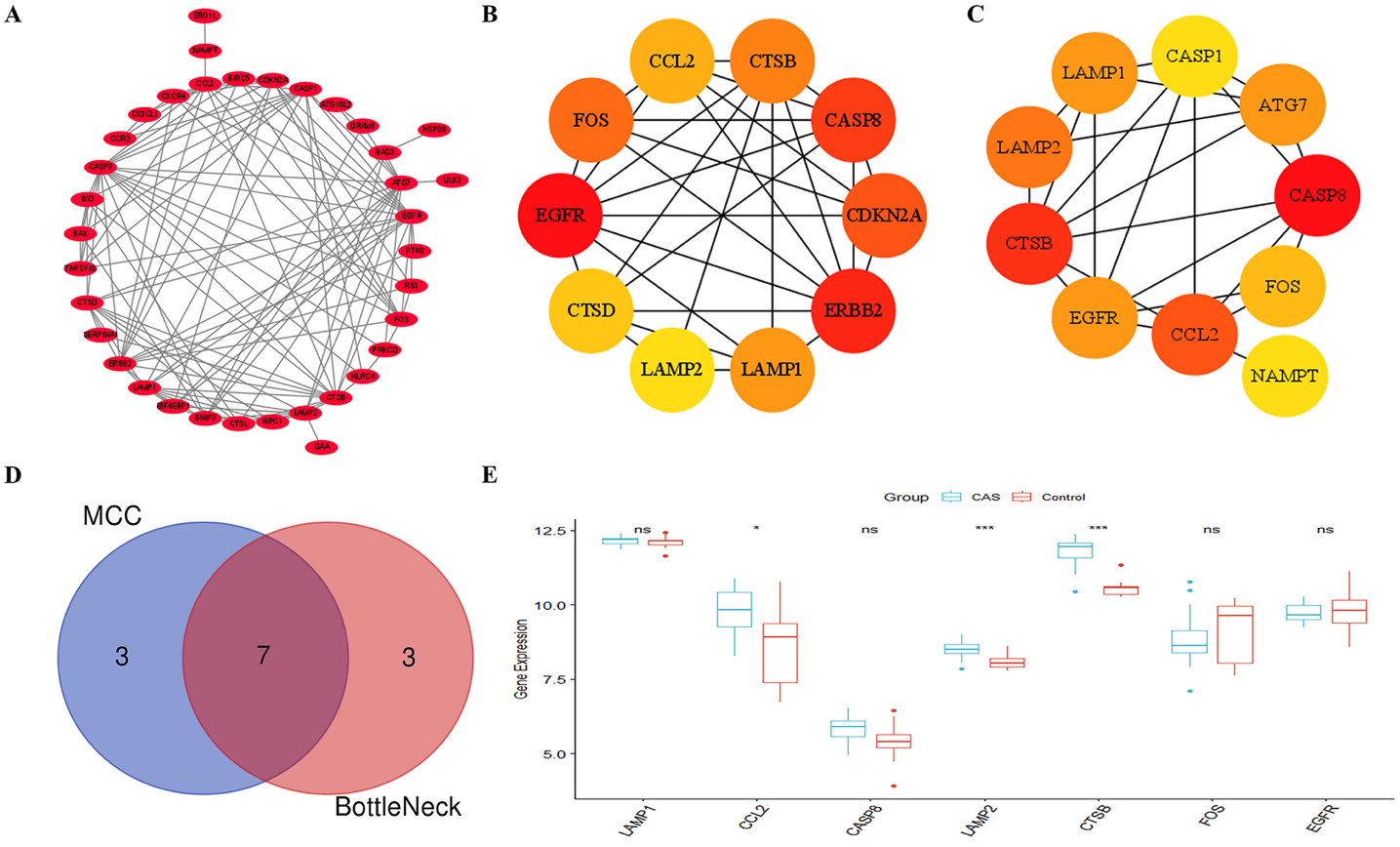

Figure 5 Identification of key CAS-related DE-ATGs. (A) The PPI network. (B) The MCC algorithm identified 10 key CAS-related DE-ATGs. (C) The BottleNeck algorithm identified 10 key CAS-related DE-ATGs. (D) Seven key CAS-related DE-ATGs were obtained by combining the MCC algorithm and BottleNeck algorithm. (E) Seven key CAS-related DE-ATGs were verified in the GSE28829 dataset. ns > 0.05; *P < 0.05; ***P < 0.001.
Full-size DOI: 10.7717/peerj.18543/fig-5

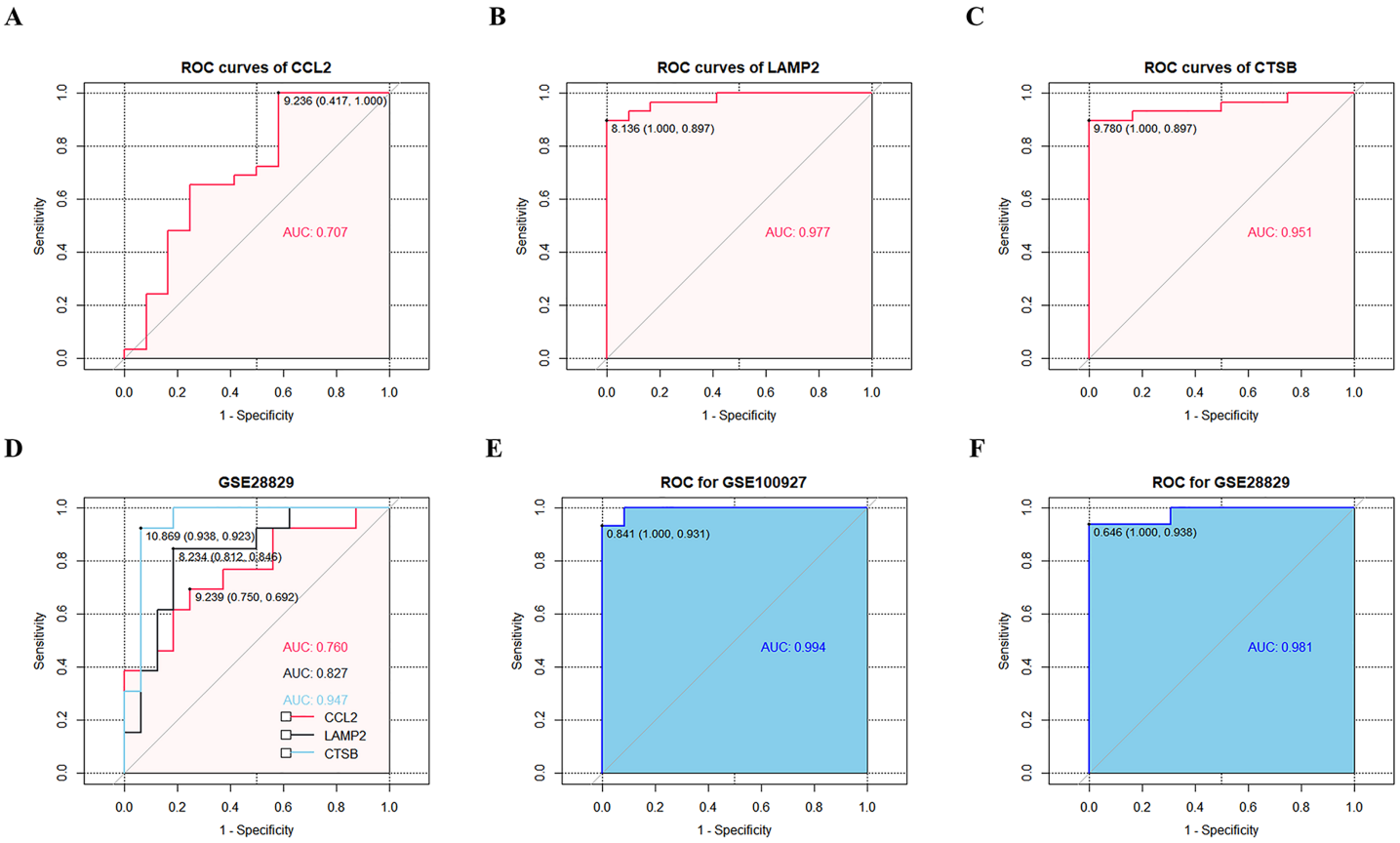

Figure 6 ROC curves of the three key CAS-related DE-ATGs in the diagnostic value and logistic regression model. ROC curves of (A) CCL2, (B) LAMP2, and (C) CTSB. (D) The GSE28829 dataset was employed as an external validation sample. (E) Logistic regression model combining three key CAS-related DE-ATGs in GSE100927. (F) Logistic regression model combining three key CAS-related DE-ATGs in GSE28829.
Full-size DOI: 10.7717/peerj.18543/fig-6

mice (Figs. 9E and 9H). This demonstrated the successful establishment of atherosclerotic mouse models. IHC staining of the aortic root also showed that the expression levels of CCL2, LAMP2, and CTSB were higher in the AS group compared with the control group (Figs. 9F, 9I–9K).

DISCUSSION

CAS is a chronic inflammatory disease characterized by accumulation of lipids and immune cells in the sub-endothelial space of the carotid artery that causes significant damage to the endothelium (*Herrero-Fernandez et al., 2019*). Several studies have demonstrated that autophagy plays an essential role in the inhibition of inflammation and cholesterol efflux (*Shao et al., 2016*; *Zhang & Zhang, 2022*). However, in-depth investigations have not been conducted regarding the role of autophagy in CAS. Therefore, in this study we investigated the role of autophagy in the progression of CAS by identifying key ATGs associated with CAS.

Firstly, we identified 41 DE-ATGs in CAS based on the transcriptome data analysis of the GSE100927 dataset (GEO database) and the human autophagy database. Functional enrichment analysis of the DE-ATGs demonstrated that these DE-ATGs were associated

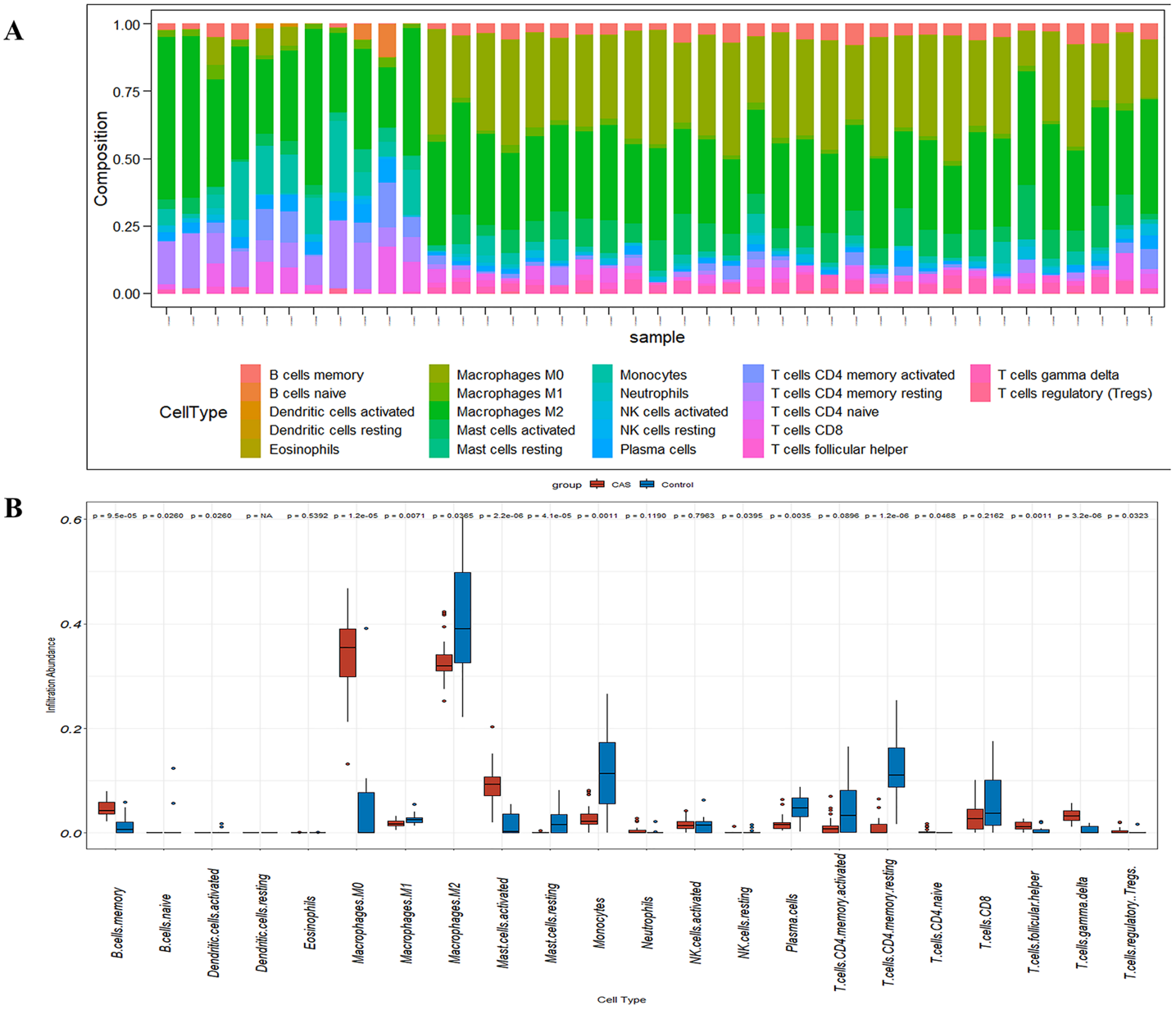

Figure 7 The fraction of 22 immune cells in CAS and control samples. (A) A barplot of 22 immune cell fractions. X-axis: GSM; Y-axis: percentage of immune cells. (B) A boxplot of 22 immune cell proportions. Full-size DOI: 10.7717/peerj.18543/fig-7

with apoptosis, autophagy, and immune activation. We further identified three key DE-ATGs (*CCL2*, *LAMP2*, and *CTSB*) that were associated with CAS. ROC curve analysis demonstrated a high diagnostic value for these three key CAS-related DE-ATGs. Moreover, these three key DE-ATGs were associated with the infiltration of various immune cells into the atherosclerotic lesions. Estimation of the lesion area in the aortic root is the standard protocol for quantitating atherosclerosis in animal models (*Song & Chen, 2021*). Therefore, we quantified the lesion areas in the AS mouse model. Western blot and qRT-PCR analysis of the *in vitro* ox-LDL-treated HUVECs and HAoSMCs was

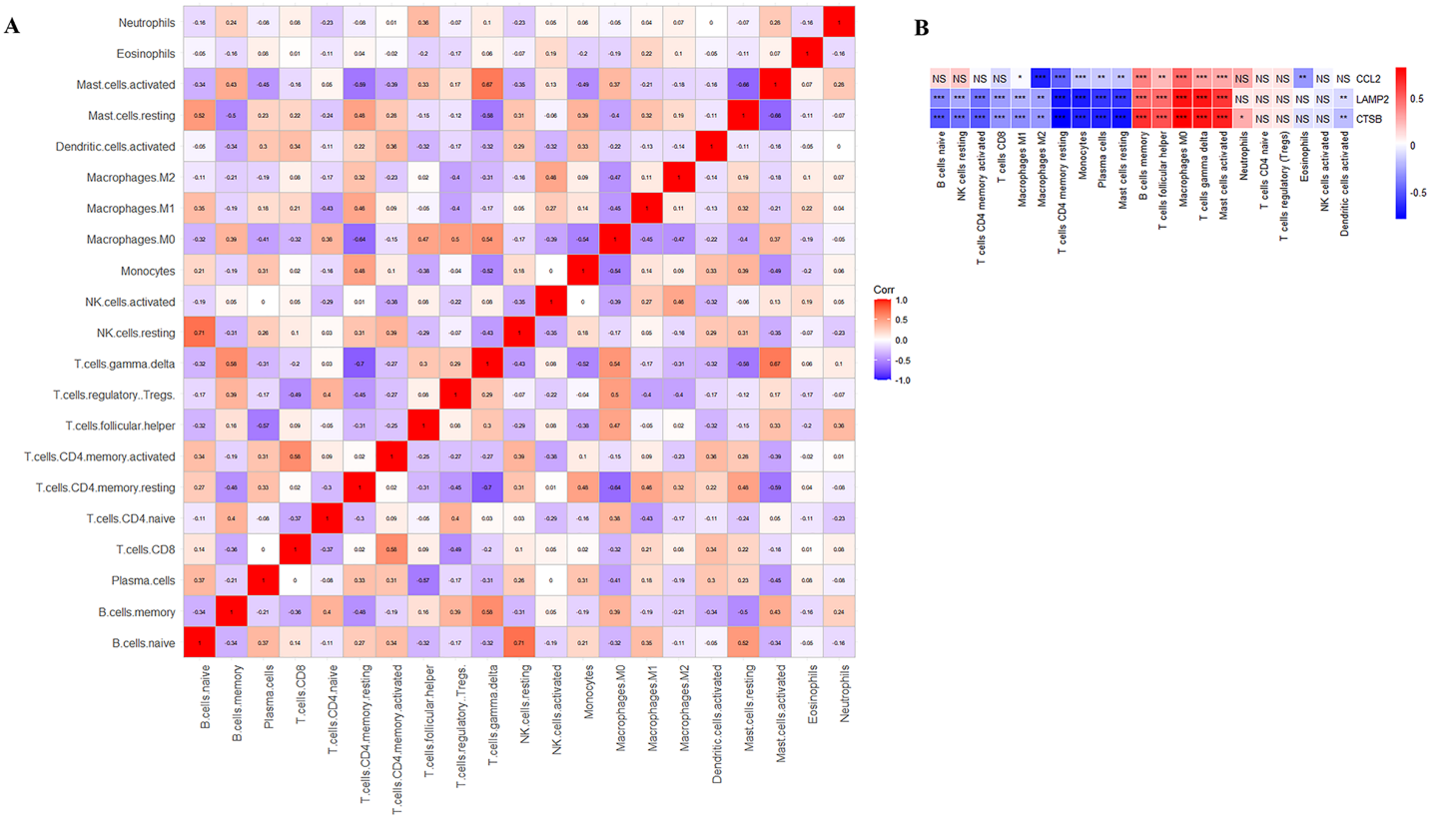

Figure 8 Correlation analysis. (A) Correlation analysis of immune cell proportions; (B) correlation analysis of immune cells and three key CAS-related DE-ATGs. ns > 0.05; *P < 0.05; **P < 0.01; ***P < 0.001. Full-size DOI: 10.7717/peerj.18543/fig-8

used to validate the high expression of these three key ATGs. IHC staining of the aortic root was used to further confirm differential expression of these three key ATGs in the CAS model mice. Cellular and animal experiments showed that *CCL2, LAMP2*, and *CTSB* were highly expressed in the AS group. Therefore, these three key ATGs are potential diagnostic biomarkers and therapeutic targets for CAS.

CC-motif chemokine ligand 2 (CCL2) plays a key role in inflammation by enhancing the migration of monocytes/macrophages, thereby regulating the development of atherosclerosis (*Singh, Anshita & Ravichandiran, 2021*). CCL2 stimulates the release of several inflammatory mediators that promote the progression of CAS (*Satonaka et al., 2015*). The CCL2-CCR2 pathway is an emerging drug target for protecting against atherosclerosis and other cardiovascular diseases by regulating inflammation (*Georgakis et al., 2022*). CCL2 expression is significantly increased by inhibiting autophagy in the ATG7-specific knockout VSMCs and mice (*Osonoi et al., 2018*). Therefore, we postulate that CCL2 may promote inflammation and ultimately lead to the development of CAS by inhibiting autophagy.

Lysosomal-associated membrane protein 2 (LAMP2) is predominantly found on lysosomal membranes and influences the formation of CAS by regulating autophagy (*Eskelinen, 2006*; *Zhang et al., 2021a*, *2021b*). LAMP2-deficient mice showed accelerated atherosclerotic progression because of increased activation of the NLRP3 inflammasome

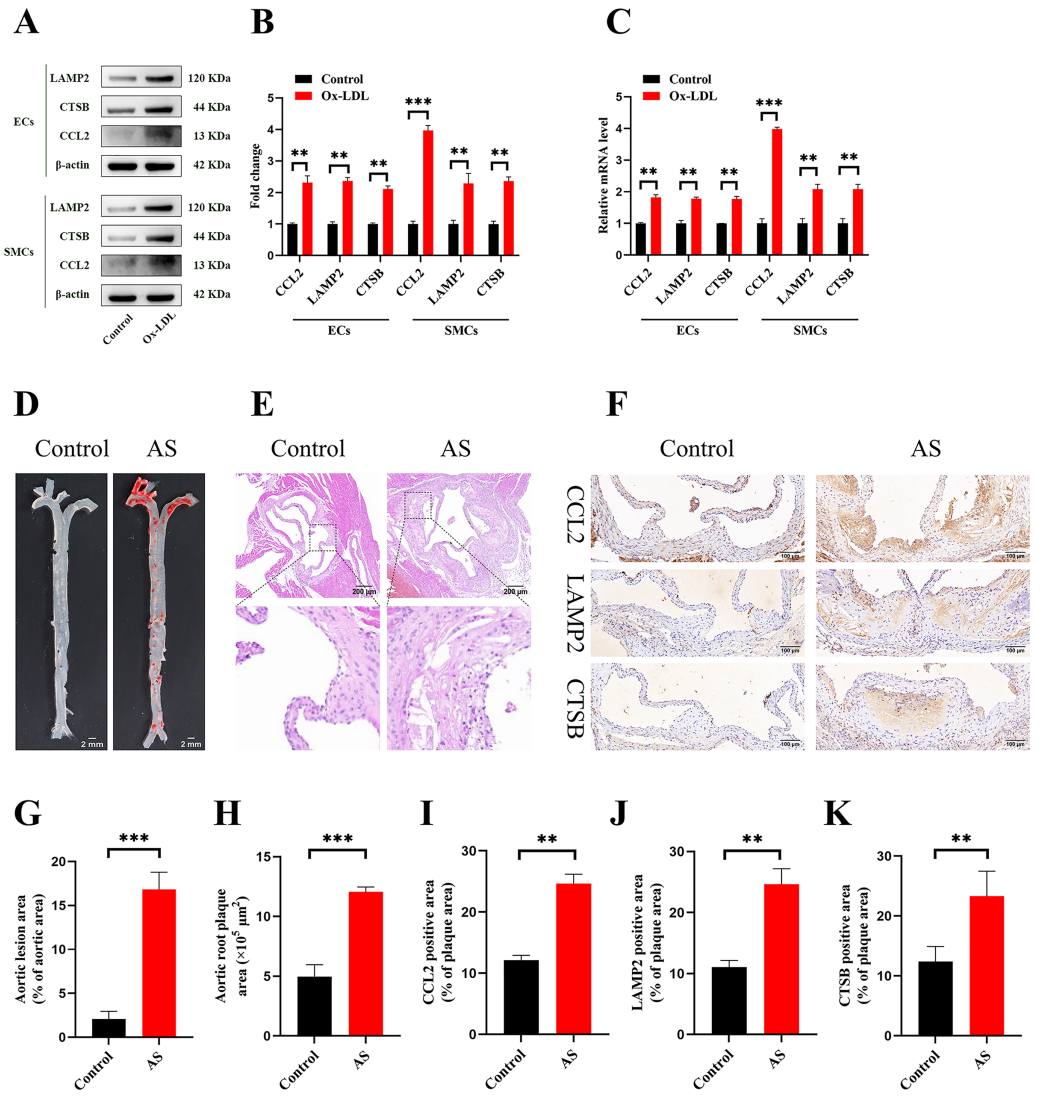

Figure 9 Vitro and vivo experiments verified the expression of three key CAS-related DE-ATGs. (A) HUVECs and HAoSMCs were incubated with ox-LDL (50 μg/mL) for 24 h or with normal medium for 24 h, and the expression of CCL2, LAMP2, and CTSB was measured by western blot (original blots are presented in Figs. S1 and S2). (B) Quantitative result of western blot. (C) QRT-PCR measured the expression of CCL2, LAMP2, and CTSB. (D) ORO staining of the entire aortas. Scale bars, 2 mm. (E) HE staining of the aortic root. Scale bars, 200 μm. (F) The aortic root was stained with antibodies against CCL2, LAMP2, and CSTB. Scale bars, 100 μm. (G) Quantification of the proportion of ORO positive area/total aortic area (%). (H) Quantitative data of the aortic root plaque area. (I–K) The percentages of CCL2, LAMP2, and CTSB positive area in the aortic root lesion. Data are presented as mean ± SD ($n = 6$). $^{*}P < 0.05$; $^{**}P < 0.01$; $^{***}P < 0.001$. Full-size DOI: 10.7717/peerj.18543/fig-9

and inflammation (*Qiao et al., 2021*). Among patients suffering from coronary heart disease, LAMP2 gene expression was significantly increased in peripheral leukocytes, suggesting that increased LAMP2 is a protective factor (*Wu et al., 2011*). Therefore, we could infer that high expression of LAMP2 would slow down the progression of CAS by suppressing inflammation through enhanced autophagy.

Cathepsin B (CTSB) is a lysosomal cysteine protease found in autolysosomes during autophagy and plays a key role in CAS (*Cai, Xu & Liu, 2024*; *Man & Kanneganti, 2016*). CTSB leads to apoptosis by promoting autophagy (*Chen et al., 2021*). The expression levels of CTSB are elevated in chronic heart disease (*Dai et al., 2021*). We postulate that CTSB-activated autophagy delays the progression of CAS by promoting cellular apoptosis in patients with CAS. Therefore, drugs that increase CTSB levels may be effective in slowing down the progression of CAS and improving the prognosis of patients with CAS.

Dysregulation of autophagy is present in atherosclerosis. Basic autophagy exerts anti-atherosclerotic effects by promoting cholesterol efflux and attenuating inflammatory responses, whereas inhibited or overstimulated autophagy exerts pro-atherosclerotic effects by inhibiting cholesterol efflux and exacerbating inflammatory responses (*Lin et al., 2021*). For example, ATG14 inhibited inflammation and atherosclerosis by promoting autophagy (*Zhang et al., 2021a*). However, ATG7 silencing in the VSMCs and mice inhibited autophagy and accelerated atherosclerotic development (*Osonoi et al., 2018*). In our study, CCL2 promotes CAS by inhibiting autophagy, whereas LAMP2 and CTSB inhibit CAS by enhancing autophagy.

CAS is a chronic inflammatory disease associated with the immune response (*Roy, Orecchioni & Ley, 2022*; *Wolf & Ley, 2019*). Single-cell sequencing data has previously confirmed significant enrichment of T cells and macrophages in the CAS plaques (*Fernandez et al., 2019*). However, the role of other immune cells needs to be clarified. We used CIBERSORT to assess the proportion of different types of immune cells in the early and advanced plaques. In the current study, the proportion of M0 macrophages and gamma delta T cells was significantly higher in the advanced plaques compared with the early plaques. This concurred with the results from previous studies that also showed higher proportions of M0 macrophages and gamma delta T cells in the atherosclerotic plaques (*Shen et al., 2021*; *Yang et al., 2021*). Previous studies have also shown that significant increase in the proportion of mast cells promotes the initiation and progression of atherosclerosis (*Bot & Biessen, 2011*; *Bot, Shi & Kovanen, 2015*). Subsequently, we demonstrated that the three key ATGs with diagnostic value were closely associated with the immune cells. Therefore, we propose that a combination of the expression levels of the key DE-ATGs and the infiltration levels of immune cells would significantly increase inflammation within the plaques in advanced CAS.

In recent years, targeted drugs have developed rapidly and are preferred for clinical use because of their therapeutic stability and low toxicity (*Yang et al., 2020*). For example, a targeted drug loaded with IL-10 mRNA inhibits the progression of atherosclerosis by suppressing inflammation (*Gao et al., 2023*). We postulate that development of targeted drugs to these key ATGs may reduce the risk of surgery and the cost of early intervention for the CAS patients. Functional analysis of the three key ATGs demonstrated that increased CCL2 expression was linked to inflammatory activation and deficient autophagy, whereas increased LAMP2 and CTSB expression was linked to activation of autophagy. This suggested that combining anti-inflammatory drugs with drugs that increase autophagy may be an effective treatment strategy for suppressing the progression of CAS.

This study has several limitations. Firstly, we analyzed only two publicly available datasets with limited samples. In the future, bioinformatics analyses of a larger number of samples and datasets are required to confirm our findings. Secondly, further experimental validation is required to confirm the changes in the immune cell type composition of the early and advanced plaques. Finally, we verified expression levels of the three key ATGs in the *in vitro* and *in vivo* experiments but did not investigate the potential mechanism of these genes in cells and tissues. So, further *in vitro* and *in vivo* experiments are necessary to confirm our findings.

CONCLUSION

We identified three key DE-ATGs (CCL2, LAMP2, and CTSB) that were linked to the formation and progression of the CAS plaques. These three key DE-ATGs were associated with the infiltration of immune cell types into the CAS plaques. *CCL2*, *LAMP2*, and *CTSB* are promising diagnostic biomarkers and therapeutic targets for patients with CAS.

ACKNOWLEDGEMENTS

We are appreciative to the GEO database for providing us with the platform and contributors to submit their valuable datasets.

ADDITIONAL INFORMATION AND DECLARATIONS

Funding

The work was sponsored by the Postgraduate Scientific Research Innovation Project of Hunan Province (No. CX20231001), the National Key Clinical Specialty Scientific Research Project (No. Z2023034) and the Natural Science Foundation of Hunan Province (No. 2023JJ30548, 2022JJ30536). The funders had no role in study design, data collection and analysis, decision to publish, or preparation of the manuscript.

Grant Disclosures

The following grant information was disclosed by the authors:
Postgraduate Scientific Research Innovation Project of Hunan Province: CX20231001.
National Key Clinical Specialty Scientific Research Project: Z2023034.
Natural Science Foundation of Hunan Province: 2023JJ30548, 2022JJ30536.

Competing Interests

The authors declare that they have no competing interests.

Author Contributions

- Tiegen Huang conceived and designed the experiments, performed the experiments, analyzed the data, prepared figures and/or tables, authored or reviewed drafts of the article, and approved the final draft.
- Chen Su performed the experiments, prepared figures and/or tables, and approved the final draft.

- Quanli Su performed the experiments, prepared figures and/or tables, and approved the final draft.
- Yali Nie analyzed the data, authored or reviewed drafts of the article, and approved the final draft.
- Zhenni Xiao performed the experiments, prepared figures and/or tables, and approved the final draft.
- Yao Tang performed the experiments, prepared figures and/or tables, and approved the final draft.
- Jiahao Wang performed the experiments, prepared figures and/or tables, and approved the final draft.
- Xiaotian Luo conceived and designed the experiments, prepared figures and/or tables, authored or reviewed drafts of the article, and approved the final draft.
- Yixin Tang conceived and designed the experiments, prepared figures and/or tables, authored or reviewed drafts of the article, and approved the final draft.

Animal Ethics

The following information was supplied relating to ethical approvals (*i.e.*, approving body and any reference numbers):

The Animal Care and Use Committee of the University of South China.

Data Availability

The following information was supplied regarding data availability:

The genomics data is available at NCBI: GSE100927 and GSE28829.

The raw data is available at figshare: Tang, Yixin (2024). Identification and validation of three diagnostic autophagy-related genes associated with advanced plaques and immune cell infiltration in carotid atherosclerosis based on integrated bioinformatics analyses. figshare. Dataset. https://doi.org/10.6084/m9.figshare.26075161.v1.

Supplemental Information

Supplemental information for this article can be found online at http://dx.doi.org/10.7717/peerj.18543#supplemental-information.

REFERENCES

Azadi R, Mousavi SE, Kazemi NM, Yousefi-Manesh H, Rezayat SM, Jaafari MR. 2021. Anti-inflammatory efficacy of Berberine Nanomicelle for improvement of cerebral ischemia: formulation, characterization and evaluation in bilateral common carotid artery occlusion rat model. *BMC Pharmacology and Toxicology* **22(1)**:54 DOI 10.1186/s40360-021-00525-7.

Bos D, Arshi B, van den Bouwhuijsen QJA, Ikram MK, Selwaness M, Vernooij MW, Kavousi M, van der Lugt A. 2021. Atherosclerotic carotid plaque composition and incident stroke and coronary events. *Journal of the American College of Cardiology* **77(11)**:1426–1435 DOI 10.1016/j.jacc.2021.01.038.

Bot I, Biessen EA. 2011. Mast cells in atherosclerosis. *Thrombosis and Haemostasis* **106(11)**:820–826 DOI 10.1160/TH11-05-0291.

Bot I, Shi GP, Kovanen PT. 2015. Mast cells as effectors in atherosclerosis. *Arteriosclerosis, Thrombosis, and Vascular Biology* **35(2)**:265–271 DOI 10.1161/ATVBAHA.114.303570.

Bravo-San Pedro JM, Kroemer G, Galluzzi L. 2017. Autophagy and mitophagy in cardiovascular disease. *Circulation Research* **120(11)**:1812–1824 DOI 10.1161/CIRCRESAHA.117.311082.

Cai Z, Xu S, Liu C. 2024. Cathepsin B in cardiovascular disease: underlying mechanisms and therapeutic strategies. *Journal of Cellular and Molecular Medicine* **28(17)**:e70064 DOI 10.1111/jcmm.70064.

Chen C, Ahmad MJ, Ye T, Du C, Zhang X, Liang A, Yang L. 2021. Cathepsin B regulates mice granulosa cells' apoptosis and proliferation in vitro. *International Journal of Molecular Sciences* **22(21)**:11827 DOI 10.3390/ijms222111827.

Chopp M, Li Y, Zhang ZG. 2009. Mechanisms underlying improved recovery of neurological function after stroke in the rodent after treatment with neurorestorative cell-based therapies. *Stroke* **40(3_suppl_1)**:S143–S145 DOI 10.1161/STROKEAHA.108.533141.

Dai J, Zhang Q, Wan C, Liu J, Zhang Q, Yu Y, Wang J. 2021. Significances of viable synergistic autophagy-associated cathepsin B and cathepsin D (CTSB/CTSD) as potential biomarkers for sudden cardiac death. *BMC Cardiovascular Disorders* **21(1)**:233 DOI 10.1186/s12872-021-02040-3.

Eskelinen EL. 2006. Roles of LAMP-1 and LAMP-2 in lysosome biogenesis and autophagy. *Molecular Aspects of Medicine* **27(5–6)**:495–502 DOI 10.1016/j.mam.2006.08.005.

Fernandez DM, Rahman AH, Fernandez NF, Chudnovskiy A, Amir ED, Amadori L, Khan NS, Wong CK, Shamailova R, Hill CA, Wang Z, Remark R, Li JR, Pina C, Faries C, Awad AJ, Moss N, Bjorkegren JLM, Kim-Schulze S, Gnjatic S, Ma'ayan A, Mocco J, Faries P, Merad M, Giannarelli C. 2019. Single-cell immune landscape of human atherosclerotic plaques. *Nature Medicine* **25(10)**:1576–1588 DOI 10.1038/s41591-019-0590-4.

Gao M, Tang M, Ho W, Teng Y, Chen Q, Bu L, Xu X, Zhang XQ. 2023. Modulating plaque inflammation via targeted mRNA nanoparticles for the treatment of atherosclerosis. *ACS Nano* **17(18)**:17721–17739 DOI 10.1021/acsnano.3c00958.

Georgakis MK, Bernhagen J, Heitman LH, Weber C, Dichgans M. 2022. Targeting the CCL2-CCR2 axis for atheroprotection. *European Heart Journal* **43(19)**:1799–1808 DOI 10.1093/eurheartj/ehac094.

Grootaert MOJ, Moulis M, Roth L, Martinet W, Vindis C, Bennett MR, De Meyer GRY. 2018. Vascular smooth muscle cell death, autophagy and senescence in atherosclerosis. *Cardiovascular Research* **114(4)**:622–634 DOI 10.1093/cvr/cvy007.

Herrero-Fernandez B, Gomez-Bris R, Somovilla-Crespo B, Gonzalez-Granado JM. 2019. Immunobiology of atherosclerosis: a complex net of interactions. *International Journal of Molecular Sciences* **20(21)**:5293 DOI 10.3390/ijms20215293.

Ke D, Ni J, Yuan Y, Cao M, Chen S, Zhou H. 2024. Identification and validation of hub genes related to neutrophil extracellular traps-mediated cell damage during myocardial infarction. *Journal of Inflammation Research* **17**:617–637 DOI 10.2147/JIR.S444975.

Kong P, Cui ZY, Huang XF, Zhang DD, Guo RJ, Han M. 2022. Inflammation and atherosclerosis: signaling pathways and therapeutic intervention. *Signal Transduction and Targeted Therapy* **7(1)**:131 DOI 10.1038/s41392-022-00955-7.

Levine B, Kroemer G. 2019. Biological functions of autophagy genes: a disease perspective. *Cell* **176(1–2)**:11–42 DOI 10.1016/j.cell.2018.09.048.

Liao X, Sluimer JC, Wang Y, Subramanian M, Brown K, Pattison JS, Robbins J, Martinez J, Tabas I. 2012. Macrophage autophagy plays a protective role in advanced atherosclerosis. *Cell Metabolism* **15(4)**:545–553 DOI 10.1016/j.cmet.2012.01.022.

Lin L, Zhang MX, Zhang L, Zhang D, Li C, Li YL. 2021. Autophagy, pyroptosis, and ferroptosis: new regulatory mechanisms for atherosclerosis. *Frontiers in Cell and Developmental Biology* **9**:809955 DOI 10.3389/fcell.2021.809955.

Lu H, Daugherty A. 2015. Atherosclerosis. *Arteriosclerosis, Thrombosis, and Vascular Biology* **35(3)**:485–491 DOI 10.1161/ATVBAHA.115.305380.

Ma Y, Gu T, He S, He S, Jiang Z. 2023. Development of stem cell therapy for atherosclerosis. *Molecular and Cellular Biochemistry* **479(4)**:779–791 DOI 10.1007/s11010-023-04762-8.

Mahapatra KK, Mishra SR, Behera BP, Patil S, Gewirtz DA, Bhutia SK. 2021. The lysosome as an imperative regulator of autophagy and cell death. *Cellular and Molecular Life Sciences* **78(23)**:7435–7449 DOI 10.1007/s00018-021-03988-3.

Man SM, Kanneganti TD. 2016. Regulation of lysosomal dynamics and autophagy by CTSB/cathepsin B. *Autophagy* **12(12)**:2504–2505 DOI 10.1080/15548627.2016.1239679.

Masuhr F, Busch M. 2004. ACST: which subgroups will benefit most from carotid endarterectomy? *Lancet* **364(9440)**:1123–1124 author reply 1125–1126 DOI 10.1016/S0140-6736(04)17091-8.

Mizushima N, Levine B. 2020. Autophagy in human diseases. *New England Journal of Medicine* **383(16)**:1564–1576 DOI 10.1056/NEJMra2022774.

Newman AM, Liu CL, Green MR, Gentles AJ, Feng W, Xu Y, Hoang CD, Diehn M, Alizadeh AA. 2015. Robust enumeration of cell subsets from tissue expression profiles. *Nature Methods* **12(5)**:453–457 DOI 10.1038/nmeth.3337.

Osonoi Y, Mita T, Azuma K, Nakajima K, Masuyama A, Goto H, Nishida Y, Miyatsuka T, Fujitani Y, Koike M, Mitsumata M, Watada H. 2018. Defective autophagy in vascular smooth muscle cells enhances cell death and atherosclerosis. *Autophagy* **14(11)**:1991–2006 DOI 10.1080/15548627.2018.1501132.

Qiao L, Ma J, Zhang Z, Sui W, Zhai C, Xu D, Wang Z, Lu H, Zhang M, Zhang C, Chen W, Zhang Y. 2021. Deficient chaperone-mediated autophagy promotes inflammation and atherosclerosis. *Circulation Research* **129(12)**:1141–1157 DOI 10.1161/CIRCRESAHA.121.318908.

Roy P, Orecchioni M, Ley K. 2022. How the immune system shapes atherosclerosis: roles of innate and adaptive immunity. *Nature Reviews Immunology* **22(4)**:251–265 DOI 10.1038/s41577-021-00584-1.

Saba L, Saam T, Jäger HR, Yuan C, Hatsukami TS, Saloner D, Wasserman BA, Bonati LH, Wintermark M. 2019. Imaging biomarkers of vulnerable carotid plaques for stroke risk prediction and their potential clinical implications. *The Lancet Neurology* **18(6)**:559–572 DOI 10.1016/S1474-4422(19)30035-3.

Satonaka H, Nagata D, Takahashi M, Kiyosue A, Myojo M, Fujita D, Ishimitsu T, Nagano T, Nagai R, Hirata Y. 2015. Involvement of P2Y12 receptor in vascular smooth muscle inflammatory changes via MCP-1 upregulation and monocyte adhesion. *American Journal of Physiology-Heart and Circulatory Physiology* **308(8)**:H853–H861 DOI 10.1152/ajpheart.00862.2013.

Shao BZ, Han BZ, Zeng YX, Su DF, Liu C. 2016. The roles of macrophage autophagy in atherosclerosis. *Acta Pharmacologica Sinica* **37(2)**:150–156 DOI 10.1038/aps.2015.87.

Shen Y, Xu LR, Tang X, Lin CP, Yan D, Xue S, Qian RZ, Guo DQ. 2021. Identification of potential therapeutic targets for atherosclerosis by analysing the gene signature related to different immune cells and immune regulators in atheromatous plaques. *BMC Medical Genomics* **14**:145 DOI 10.1186/s12920-021-00991-2.

Singh S, Anshita D, Ravichandiran V. 2021. MCP-1: function, regulation, and involvement in disease. *International Immunopharmacology* **101(2)**:107598 DOI 10.1016/j.intimp.2021.107598.

Song T, Chen WD. 2021. Berberine inhibited carotid atherosclerosis through PI3K/AKTmTOR signaling pathway. *Bioengineered* **12(1)**:8135–8146 DOI 10.1080/21655979.2021.1987130.

Stary HC, Chandler AB, Dinsmore RE, Fuster V, Glagov S, Insull W Jr, Rosenfeld ME, Schwartz CJ, Wagner WD, Wissler RW. 1995. A definition of advanced types of atherosclerotic lesions and a histological classification of atherosclerosis. A report from the committee on vascular lesions of the council on arteriosclerosis, American heart association. *Circulation* **92**:1355–1374 DOI 10.1161/01.cir.92.5.1355.

Steenman M, Espitia O, Maurel B, Guyomarch B, Heymann MF, Pistorius MA, Ory B, Heymann D, Houlgatte R, Gouëffic Y, Quillard T. 2018. Identification of genomic differences among peripheral arterial beds in atherosclerotic and healthy arteries. *Scientific Reports* **8**:3940 DOI 10.1038/s41598-018-22292-y.

Tedgui A, Mallat Z. 2006. Cytokines in atherosclerosis: pathogenic and regulatory pathways. *Physiological Reviews* **86(2)**:515–581 DOI 10.1152/physrev.00024.2005.

Wolf D, Ley K. 2019. Immunity and Inflammation in Atherosclerosis. *Circulation Research* **124(2)**:315–327 DOI 10.1161/CIRCRESAHA.118.313591.

Wu G, Huang J, Wei G, Liu L, Pang S, Yan B. 2011. LAMP-2 gene expression in peripheral leukocytes is increased in patients with coronary artery disease. *Clinical Cardiology* **34(4)**:239–243 DOI 10.1002/clc.20870.

Yamamoto H, Zhang S, Mizushima N. 2023. Autophagy genes in biology and disease. *Nature Reviews Genetics* **24(6)**:382–400 DOI 10.1038/s41576-022-00562-w.

Yang Y, Cai Y, Zhang Y, Yi X, Xu Z. 2021. Identification of molecular subtypes and key genes of atherosclerosis through gene expression profiles. *Frontiers in Molecular Biosciences* **8**:628546 DOI 10.3389/fmolb.2021.628546.

Yang X, Pan Z, Choudhury MR, Yuan Z, Anifowose A, Yu B, Wang W, Wang B. 2020. Making smart drugs smarter: the importance of linker chemistry in targeted drug delivery. *Medicinal Research Reviews* **40(6)**:2682–2713 DOI 10.1002/med.21720.

Zhang H, Ge S, Ni B, He K, Zhu P, Wu X, Shao Y. 2021a. Augmenting ATG14 alleviates atherosclerosis and inhibits inflammation via promotion of autophagosome-lysosome fusion in macrophages. *Autophagy* **17(12)**:4218–4230 DOI 10.1080/15548627.2021.1909833.

Zhang Z, Yue P, Lu T, Wang Y, Wei Y, Wei X. 2021b. Role of lysosomes in physiological activities, diseases, and therapy. *Journal of Hematology & Oncology* **14(1)**:79 DOI 10.1186/s13045-021-01087-1.

Zhang Y, Zhang H. 2022. Identification of biomarkers of autophagy-related genes between early and advanced carotid atherosclerosis. *International Journal of General Medicine* **15**:5321–5334 DOI 10.2147/IJGM.S350232.

Zhu H, Hu S, Li Y, Sun Y, Xiong X, Hu X, Chen J, Qiu S. 2022. Interleukins and ischemic stroke. *Frontiers in Immunology* **13**:828447 DOI 10.3389/fimmu.2022.828447.